A COLLECTION OF TECHNICAL PAPERS

Part 1

10th AIAA Applied Aerodynamics Conference

June 22-24, 1992/Palo Alto, CA

AERODYNAMIC SHAPE OPTIMIZATION OF HYPERSONIC CONFIGURATIONS INCLUDING VISCOUS EFFECTS

George S. Dulikravich [1] and Scott G. Sheffer [2]
Department of Aerospace Engineering, 233 Hammond Building
The Pennsylvania State University, University Park, PA 16802, USA

ABSTRACT

A new method has been developed to optimize arbitrary (non-axisymmetric) hypersonic configurations in terms of combined aerodynamic wave drag and viscous drag minimization, while maintaining the initial volume and length of the vehicle. Because of the large number of flow analysis evaluations required by this optimization algorithm, a fast and accurate modified Newtonian flow theory and a modified boundary layer approximation were used. This shape optimization method utilized either a surface fitted Fourier series to represent the geometry of the vehicle or an independent point-motion algorithm for each surface point. In either case, the coefficients of the Fourier series or the spatial locations of the points defining each cross section were varied. A numerical optimization algorithm based on a quasi-Newton gradient search concept was used to determine the new optimal configuration. Four different configurations were optimized: cone, stubby wing, four-pointed star, and a Space Shuttle-like winged configuration. Numerical results indicate a significant decrease in aerodynamic wave drag for simple and complex configurations at a relatively low computing cost. In the case of a cone, the results agreed well with known analytical optimum ogive shapes. The procedure is capable of accepting more complex flow field analysis codes and of constraining parts of the configuration.

NOMENCLATURE

A	= area of a panel on the body surface
A_k, B_k	= coefficients of Fourier trigonometric series for coordinates at cross section i
C_f	= skin friction coefficient
C_p	= surface pressure coefficient
C_{po}	= stagnation pressure coefficient
F	= aerodynamic force applied to a panel
FAC	= percentage change in design variable
K	= number of terms in the Fourier series
M_∞	= free stream Mach number
M_n	= normal component of Mach number
$\hat{n}$	= unit normal to the body surface
p	= static pressure at a point
p_∞	= free stream static pressure
R	= specific gas constant
r	= recovery factor
Re	= Reynolds number
S	= least squares summation
s	= body cross section contour-following coordinate
$\bar{s}$	= normalized body cross section contour-following coordinate
T	= temperature
u	= velocity
x	= Cartesian coordinate along the axis
y, z	= Cartesian coordinates of a contour point at cross section i
β	= oblique shock angle
γ	= specific heat ratio of the gas
μ	= coefficient of viscosity
Σ	= summation
θ_{le}	= half angle of the body
θ_n	= angle between free stream and normal to the surface of a vehicle

Subscripts

aw	= adiabatic wall
b	= behind the oblique shock
e	= boundary layer edge
i	= i^{th} cross section of the vehicle
j	= j^{th} point of a cross section contour
le	= leading edge
k	= k^{th} coefficient of a Fourier trigonometric series
w	= wall
x	= streamline direction
*	= reference quantity
∞	= free stream value

INTRODUCTION

Although optimization of axisymmetric hypersonic bodies has been accomplished in the past [1,2], the aerodynamic drag minimization of an arbitrary hypersonic vehicle has not been attempted

[1]Associate Professor. Associate Fellow AIAA.
[2]Research Assistant. Student Member AIAA.

[3] until recently [4]. The objective of this paper is to present an optimization procedure for arbitrarily shaped hypersonic vehicles. While there are certainly some limitations of the methodologies used in this paper, it demonstrates that optimization of numerous variables can indeed be done and that this can be applied to complex configurations.

In hypersonic flow ($M_\infty > 5.0$), the flow around an object may be modeled using an impact theory. In this theory, oncoming particles strike the surface of the object and impart the normal component of their momentum to that body. Classical Newtonian flow theory has been shown to approach reality when the free stream Mach number approaches infinity and the value of the ratio of specific heats approaches $\gamma = 1$ [5]. Modified Newtonian theory has been shown to be quite satisfactory for predicting the aerodynamic forces and moments on a body [6]. Modified Newtonian theory has the main advantage of being extremely simple, accurate [7] and fast when faced with the thousands of flow field calculations needed in an optimization problem of this scope. Because of the use of modified Newtonian theory, it was implicitly assumed that the flow field was inviscid.

In this study, modified Newtonian impact flow theory was used with a modified Newtonian constrained search optimization routine [8] to obtain vehicle shapes which had significantly lower wave drag in hypersonic flow. In the first part of the study, cross section coordinates of the body were represented with curve-fitted Fourier series. Curve-fitted Chebyshev series [9] were initially considered, but it was found that the Fourier series represented complex shapes, such as a Space Shuttle configuration, better than the Chebyshev series. The coefficients of the Fourier series, one set representing the y coordinate and one set representing the z coordinate (Fig. 1), then became the design variables that were fed to the optimization routine. The optimization routine sequentially perturbed each of the coefficients by a small amount and determined the new shape that reduced wave drag while keeping the volume and length of the vehicle constant.

In the second part of the study, the y and z coordinates of the vehicle's cross section were used as the design variables directly. Again, the optimization routine perturbed separately each of the coordinates at each of the cross section contour points. Then, it combined the changes into a new shape with lower wave drag while still honoring the constraints of constant volume and constant length of the vehicle.

NUMERICAL MODELS

The first part of this investigation used a least squares Fourier series curve fit to represent the y and z coordinates of each half cross section, i, that is,

$$y_{ij} = \sum_{k=1}^{K} A_{ki} \cos[(k-1)\pi \bar{s}_{i,j}] \tag{1}$$

$$z_{ij} = \sum_{k=1}^{K} B_{ki} \sin[k\pi \bar{s}_{i,j}] \tag{2}$$

where $\bar{s}_{i,j}$ was a normalized contour-following coordinate (Fig. 1) such that

$$s_{i,j} = s_{i,j-1} + \sqrt{(y_{i,j} - y_{i,j-1})^2 + (z_{i,j} - z_{i,j-1})^2}$$

$$\text{and} \quad \bar{s}_{i,j} = \frac{s_{i,j}}{s_{i,jmax}} \tag{3}$$

A_{ki} was determined from the least squares fit of the Fourier series

$$S_i = \sum_{j=1}^{jmax} \left(\sum_{k=1}^{K} (A_{ki} \cos[(k-1)\pi \bar{s}_{i,j}]) - y_{i,j} \right)^2$$

$$\text{and} \quad \frac{\partial S_i}{\partial A_{ki}} = 0. \tag{4}$$

The coefficients B_{ki} were determined in a similar way. Since it was assumed that the vehicle had a vertical plane of symmetry, the z-coordinates of the first (j=1) and the last (j=jmax) point of each half cross section were always zero thus ensuring symmetry across the y-axis.

The local surface pressure coefficient, $C_{p,ij}$, was calculated by the use of modified Newtonian impact flow theory [6], which states that

$$C_{p,ij} = C_{po} \cos^2\theta_{n,ij} \tag{5}$$

where $\theta_{n,ij}$ is the angle between the free stream and the normal to the surface. The stagnation pressure coefficient, C_{po}, is given by

$$C_{po} = \frac{2}{\gamma M_\infty^2}\left[\left(\frac{\gamma+1}{2\gamma M_\infty^2 - \gamma + 1}\right)^{\frac{1}{\gamma-1}} \left(\frac{\gamma+1}{2} M_\infty^2\right)^{\frac{\gamma}{\gamma-1}} - 1\right] \tag{6}$$

The pressure on a given segment of the body may then be calculated from the rearranged formula for $C_{p,ij}$, that is

$$p_{ij} = p_\infty + \frac{1}{2} C_{p,ij} \gamma p_\infty M_\infty^2 \quad (7)$$

The aerodynamic force on each surface panel is found from

$$\bar{F}_{ij} = - p_{ij} A_{ij} \hat{n}_{ij} \quad (8)$$

so that the resultant force on the entire body is obtained by summing all of the panel forces

$$\bar{F}_{total} = \sum_{ij} F_{ij} \quad (9)$$

Aerodynamic wave drag was then the x-component of the resultant aerodynamic force.

The optimization algorithm perturbed each of the Fourier coefficients to obtain a slightly different shape. After perturbing all of the coefficients and analyzing these new perturbed shapes, the optimization algorithm combined the changes into a new shape that met the constraints of constant volume and constant length, but which had a reduced aerodynamic wave drag.

The second part of the study was exactly the same as the first part, except that instead of working with the Fourier series coefficients, the y and z coordinates of the cross sections' points were perturbed directly and independently of each other.

VISCOSITY EFFECTS

Hypersonic drag due to viscosity effects should be accounted for when minimizing the overall drag [3,10,11]. We have incorporated the effects of viscosity via a boundary layer which was applied in a locally two-dimensional strip fashion. This boundary layer was either fully laminar or fully turbulent. Our formulation is somewhat different from that used in the APAS code [11]. Specifically, we used local (variable) values for the adiabatic wall temperature, T_{AW}, rather than a constant value based on the free stream Mach number [11]. The procedure takes into account the fact that there is some type of an oblique shock wave at a leading edge of a typical hypersonic configuration. Fluid particles that enter the boundary layer and those that move along the boundary layer must pass through the shock wave. We do not know the shock angle *a priori*, since the initial configuration is to be changed during the optimization process. In addition, we cannot compute the oblique shock angle accurately using simple empiricism because the shock is three-dimensional and at best conical. Thus, we have decided to approximate the problem as that of a two-dimensional planar oblique shock attached to a wedge of a known wedge angle.

Given the values of γ, p_∞, T_∞, θ_{le} and M_∞ it is then easy to determine the oblique shock angle β as

$$\tan \theta_{le} = 2 \cot \beta \frac{M_\infty^2 \sin^2\beta - 1}{M_\infty^2(\gamma + \cos 2\beta) + 2} \quad (10)$$

The normal component of the Mach number ahead of the leading edge shock is

$$M_{\infty n} = M_\infty \sin \beta. \quad (11)$$

Then, the normal component of the Mach number behind the leading edge shock is obtained from

$$M_{bn}^2 = \frac{1 + \frac{\gamma-1}{2} M_{\infty n}^2}{\gamma M_{\infty n}^2 - \frac{\gamma-1}{2}} \quad (12)$$

Pressure behind the leading edge oblique shock is then

$$\frac{p_b}{p_\infty} = 1 + \frac{2\gamma}{\gamma+1}(M_{\infty n}^2 - 1) \quad (13)$$

while the Mach number behind the leading edge shock is

$$M_b = \frac{M_{bn}}{\sin(\beta - \theta_{le})} . \quad (14)$$

From the modified Newtonian theory algorithm we obtain local surface values of C_p. From the definition of local $C_{p,ij}$ we get

$$p_{ij} = p_\infty (1 + \gamma C_{p,ij} M_\infty^2/2) \quad (15)$$

Assuming that the inviscid part of the flow behind the leading edge shock is isentropic, we can determine the local values of the Mach number from

$$\frac{p_{ij}}{p_b} = \left[(1 + \frac{\gamma-1}{2} M_\infty^2)/(1 + \frac{\gamma-1}{2} M_{ij}^2) \right]^{\frac{\gamma}{\gamma-1}} \quad (16)$$

The local temperature at the edge of the boundary layer is

$$T_{ij} = T_o (1 + \frac{\gamma-1}{2} M_{ij}^2)^{-1} \quad (17)$$

Then, the local adiabatic wall temperature, $T_{AW,ij}$, is

$$\frac{T_{AW,ij}}{T_{ij}} = 1 + r\frac{\gamma-1}{2}M_{ij}^2 \qquad (18)$$

Properties are evaluated at a reference temperature [11] which is given as

$$T^*_{ij} = a_1 T_W + a_2 T_{AW,ij} + (1 - a_1 - a_2) T_{ij} \qquad (19)$$

where $a_1 = 0.50$, $a_2 = 0.22$ [10] and T_W was assumed to be 600 K. The viscosity coefficient was determined from Sutherland's Law

$$\frac{\mu^*_{ij}}{\mu_\infty} = \left[\frac{T^*_{ij}}{T_\infty}\right]^{1.5} \frac{T_\infty + C}{T^*_{ij} + C} \qquad (20)$$

where C = 110 K. Reynolds number based on the streamline coordinate is then

$$Re^*_x = \frac{\rho^* u_e S_x}{\mu^*} \qquad (21)$$

where $\rho^* = RT^*_{ij}/p_{ij}$ and u_e is

$$u_e = M_{ij}\sqrt{\gamma R T_{ij}} \qquad (22)$$

The skin friction coefficient for a laminar boundary layer on a flat plate is given by

$$C_f = \frac{0.664}{\sqrt{Re^*_x}} \qquad (23)$$

while the skin friction coefficient for a turbulent boundary layer on a flat plate is

$$C_f = \frac{0.88\,(\ln Re^*_x - 2.3686)}{(\ln Re^*_x - 1.5)^3} \qquad (24)$$

Local surface shear stress is then calculated from

$$\tau_w = \frac{C_f \rho^* u_e^2}{2} \qquad (25)$$

RESULTS

Based on modified Newtonian impact theory, a hypersonic analysis code was developed for arbitrary three-dimensional configurations. It was combined with the modified Newtonian search algorithm published in the book by Pshenichny and Danilin [8]. Boundary layer effects were incorporated in the flow field analysis code using the formulas given above.

Four test cases were run for the inviscid part of this study. They consisted of a straight cone having circular cross section shapes, a straight cone having a four pointed star as a cross section, a stubby-wing shaped body and a Space Shuttle-like configuration. All cases were run at an angle of attack of 0°, a specific heat ratio of $\gamma = 1.4$ and a free stream Mach number of $M_\infty = 10$. Notice that the values for γ and M_∞ appear in C_{po} which may be factored out of the pressure coefficient ratio thus affecting the numerical amount of inviscid drag, but not the qualitative amount of the inviscid drag. The x-axis for each case was chosen to coincide with the long axis of the body. The y and z-axes were then mutually perpendicular to the x-axis.

Fourier Series Algorithm: For the initial part of the study, twenty terms in a Fourier series for y and z coordinates were used for seven cross sections. Twenty terms were chosen because this amount was able to represent the geometries of all four test cases, including the complex Space Shuttle shape. Only six of the cross sections were allowed to deform; the nose cross section was kept constant to serve as a tip. Thus there were 6 x 20 x 2 = 240 design variables. Twenty-five points were used per cross section; thus, the half body was discretized into 6 x 24 = 144 panels. FAC, the percent perturbation of A_{mi} and B_{mi} in the optimization algorithm, was set equal to 5%.

For the case of a right circular cone (Fig. 2), after a total of 43 iterations, the program converged to an ogive configuration that had 47.96% less wave drag than the original conical configuration. Note that horizontal and vertical symmetry were maintained.

The next shape tested was a four pointed star configuration (Fig. 3). The aerodynamic wave drag of this shape was reduced by 39.16% after 43 iterations. This case did not converge due to "fishtailing" of the fins and was terminated just before such fishtailing occurred. Note the streaking near the nose and the thinning of the points on the last cross section. Also, notice that vertical and horizontal symmetry were maintained and the fin planforms assumed an ogiving shape.

The third shape optimized was that of a "stubby wing" configuration (Fig. 4). The wave drag was reduced by 64.62% when the algorithm converged after 53 iterations while preserving cross-

axis symmetry. Again, note the streaking toward the nose and the smooth appearance of four small fins along the wing tip line.

The fourth test case was that of a Space Shuttle configuration (Fig. 5). After 22 iterations, the wing surface crossed itself and the process was terminated. Aerodynamic wave drag was reduced by 18.52%. With careful scrutiny, one can notice that the centerbody has become ogived, the wing thickness has been reduced, the wing roots have become filleted, and the underside of the fuselage has been reduced in size.

The convergence histories (Fig. 6) indicate that the general trend is a monotonic decrease in the inviscid wave drag. Table 1 shows the final drag reduction in addition to the number of analysis calls and total optimization iteration cycles.

Point-Motion Algorithm: For the point-motion algorithm, 21 points per half cross section were used. Only six cross sections were analyzed due to computer storage limitations. With only five cross sections being active, this yielded 2 x 5 x 21 = 210 design variables and 5 x 20 =100 surface panels per half cross section. FAC for this algorithm was set to 0.1%.

Numerical optimization of a straight circular cone resulted in an ogive shape with axisymmetry successfully maintained. After 49 iterations, the shape converged to that of Fig. 2 with a corresponding decrease in drag of 45.37%.

The second shape was the four pointed star. With the point-motion algorithm, the shape converged after 35 iterations to that pictured in Fig. 3. There was a reduction of drag of 34.65%. As in the case of the circular cone, symmetry was maintained across both the y and z-axes while the fin planforms exhibited significant ogiving. The resulting shape is very similar to that obtained by the coefficient algorithm.

The next shape optimized was the "stubby wing." The fin tips, after 24 iterations, crossed themselves and the process was terminated. However, a decrease of 40.58% of the original wave drag was achieved just before the shape cross-over. The development of the fins along the side of the vehicle (Fig. 4) and streaks near the nose are practically identical to those developed when using the coefficient algorithm. Once again, symmetry was maintained.

The final case for the point motion algorithm was the Space Shuttle vehicle (Fig. 5). Similar to the case in the coefficient algorithm, the wing eventually crossed itself and the run was terminated. A decrease in drag of 27.38% was found after 16 iterations preceding the cross-over.

For the point-motion algorithm, the convergence histories (Fig. 7) indicate a monotonic decrease in wave drag for all four test configurations. The total reduction in wave drag for the four test configurations when using the point-motion algorithm is summarized in Table 2.

A comparison (Figs. 8 and 9) of the numerically optimized ogive shapes with analytically optimal ogives obtained by Sears and Haack and by von Karman [12] demonstrates the reliability and accuracy of the numerical optimization algorithms.

Viscosity effects: To test the optimization algorithm with the effects of viscosity, a conical projectile of length 10 m and 15° cone half angle was tested at an altitude of 25 km and a flight Mach number of $M_\infty = 10$ while assuming that $\gamma = 1.4$. The corresponding ambient conditions were $T_\infty = 221.552$ K, $p_\infty = 2607.7$ Pa and $\mu_\infty = 14.484 \times 10^{-6}$ kg m^{-1} s^{-1}.

The optimization was performed using an inviscid modified Newtonian flow analysis algorithm until the initially conical shape converged to an optimal shaped ogive (Fig. 10). Notice that the numerically optimized shape resembles very accurately the analytically optimal ogive shape of von Karman (Fig. 11).

A laminar boundary layer computation was then activated over the entire length of the body for several additional optimization cycles. The addition of the laminar boundary layer accounted for an increase of 3.8% over the optimum inviscid drag (Fig. 12). The optimal shape resulting from the laminar boundary layer computations was practically identical to the inviscid optimal shape which in turn resembled the von Karman analytically optimal shape (Fig. 10 and Fig. 11).

When a turbulent boundary layer was activated over the entire length of the already optimized inviscid body, the total drag increased significantly (over 80% of the optimal inviscid drag). After several additional optimization cycles, the combined drag was reduced to 85% of the original inviscid drag (Fig. 12). Again, it is interesting to note that the optimal ogive shapes with laminar and turbulent boundary layers did not differ significantly (Fig. 10 and Fig. 11) from each other and from the analytically optimal inviscid von Karman body. Notice that the Sears-Haack analytically optimized body has a different shape from the von Karman optimal ogive because it was developed for slender bodies.

CONCLUSIONS

Two procedures, a coefficient algorithm and a point-motion algorithm, for aerodynamically optimizing arbitrarily shaped hypersonic vehicles have been shown to significantly reduce aerodynamic wave drag while keeping the vehicle's volume and length constant. Both formulations are fast only because a modified Newtonian flow theory was used as the flow field analysis algorithm. The addition of

viscous effects via a boundary layer approximation yielded insignificant geometric changes on simple ogive-type bodies and compared very closely with analytically optimized inviscid shapes obtained by von Karman. These optimization algorithms represent effective preliminary design tools for optimization of three-dimensional hypersonic configurations. The point motion algorithm can be used to keep parts of the original vehicle fixed, such as cabin size or wing thickness, during the optimization. More sophisticated flow field solvers that include viscosity and the effects of heat transfer could be substituted in place of the modified Newtonian flow theory and boundary layer approximations during the final stages of the optimization.

ACKNOWLEDGEMENTS

The second author would like to thank Penn State's Space Propulsion Engineering Research Center, the Penn State CFD Studies Program and the ICIDES project for financial support. Many thanks are due to Mr. Florian Sobieczky for his invaluable assistance in producing the graphics for this paper. The authors would also like to thank Apple Computer, Inc. for their donated equipment.

REFERENCES

1. Dulikravich, G. S, Buss, R. N., Strang, E. J. and Lee, S., "Aerodynamic Shape Optimization of Hypersonic Missiles", AIAA Paper 90-3073, Proc. of the AIAA 8th Applied Aerodyn. Conf., Portland, OR, August 20-22, 1990.

2. Lee, J. and Mason, W. H., "Development of an Efficient Inverse Method for Supersonic and Hypersonic Body Design", AIAA Paper 91-0395, 29th Aerospace Sciences Meeting, Reno, Nevada, January 7-10, 1991.

3. Blankson, I., "Hypersonic Waveriders: State of the Concept", AIAA Paper 91-0529, AIAA AE erospace Sciences Meet., Reno, NV , Jan. 7-10, 1991.

4. Dulikravich, G.S. and Sheffer, S.G., "Aerodynamic Shape Optimization of Arbitrary Hypersonic Vehicles", Proc. of 3rd Internat. Conf. on Inverse Design Concepts and Optimizat. in Eng. Sci. (ICIDES-III), Edt: G.S. Dulikravich, Washington, D.C., Oct. 23-25, 1991.

5. Anderson, J. D. Jr., Hypersonic and High Temperature Gas Dynamics, McGraw-Hill, New York, 1989.

6. Cox, R.N. and Crabtree, L.F., Elements of Hypersonic Aerodynamics, Academic Press, New York, 1965.

7. Geiger, R. E., "Experimental Lift and Drag of a Series of Glide Configurations at Mach Numbers 12.6 and 17.5," *Journal of Aerospace Sciences*, April 1962, pp. 410-419.

8. Pshenichny, B. N and Danilin, Y. M., Numerical Methods in Extremal Problems, MIR Publishers, Moscow, 1969.

9. Kuo, S. S., Computer Applications of Numerical Methods, Addison-Wesley Publishing Company, Inc., Philippines, 1972.

10. Brown, L.B., "Axisymmetric Bodies of Minimum Drag in Hypersonic Flow," Univ. of Texas at Austin Report U-Tex-EMRL-TR-1016, July 1967.

11. Cruz, C.I. and Engelund, W.C., "Enhancements to the High Speed Convective Heating and Viscous Drag Prediction Techniques of the Aerodynamic Preliminary Analysis System (APAS)", AIAA paper 91-1435, AIAA 26th Thermophysics Conference, Honolulu, HI, June 24-26, 1991

12. Ashley, H. and Landahl, M., Aerodynamics of Wings and Bodies, Addison-Wesley Publishing Company, Inc., Reading, Massachusetts, 1965.

Coefficient Test Case	Drag Reduction (%)	Number of Optimization Cycles	Number of Analysis Calls
Cone	47.96	43	10493
Star	39.16	43	10493
Stubby wing	64.62	53	12689
Space Shuttle	18.52	22	5125

Table 1. Drag reduction, number of optimization cycles and analysis calls for the four test cases using algorithm based on Fourier series representation of cross-section shapes (inviscid calculations).

Point-Motion Test Case	Drag Reduction (%)	Number of Optimization Cycles	Number of Analysis Calls
Cone	45.37%	49	10273
Star	34.65	35	7277
Stubby wing	40.58	24	4923
Space Shuttle	27.38	16	3211

Table 2. Drag reduction, number of optimization cycles and analysis calls for the four test cases using point-motion algorithm (inviscid calculations).

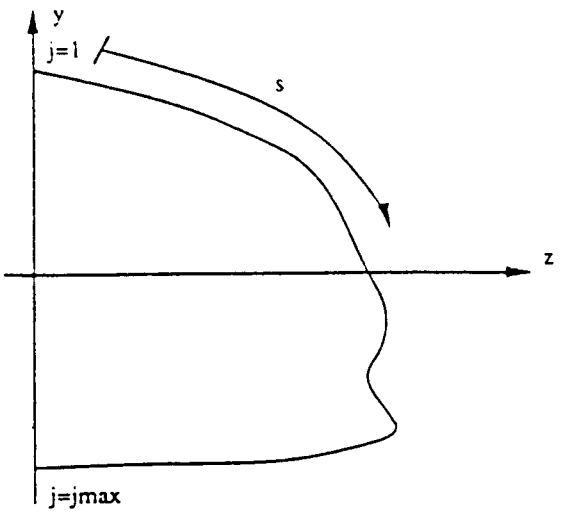

Figure 1. Cross section contour-following coordinate.

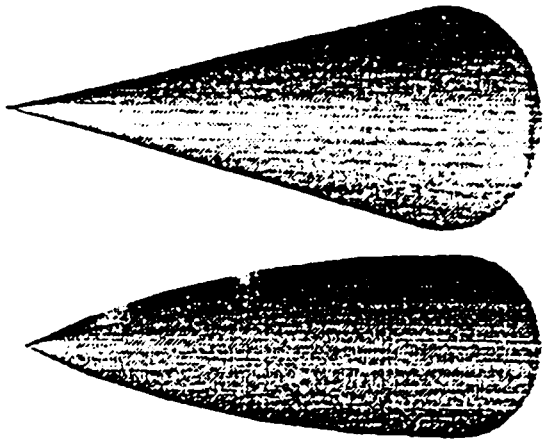

Figure 2. Straight circular cone shape; Fourier coefficient algorithm: a) initial shape, b) final shape.

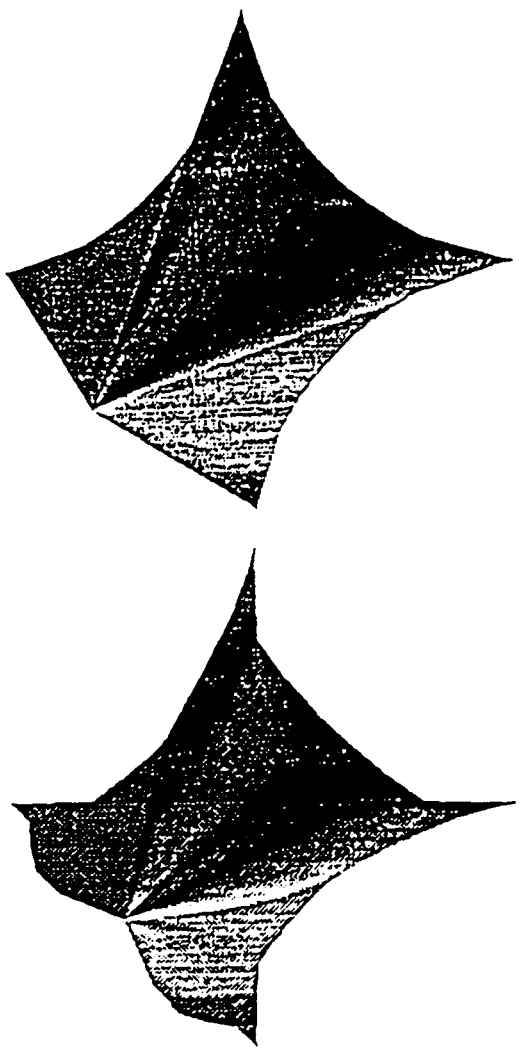

Figure 3. Four pointed star shape; Fourier coefficient algorithm: a) initial shape, b) final shape.

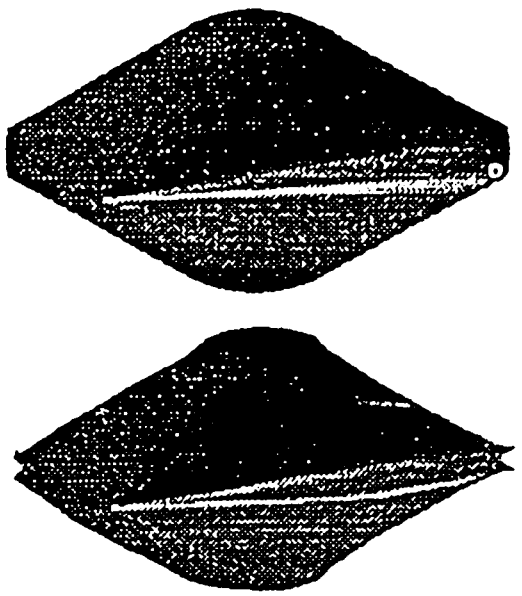

Figure 4. Stubby wing shape; Fourier coefficient algorithm: a) initial shape, b) final shape.

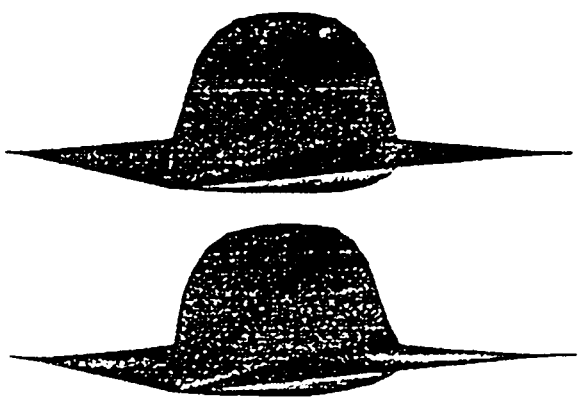

Figure 5. Space Shuttle-like shape; Fourier coefficient algorithm: a) initial shape, b) final shape.

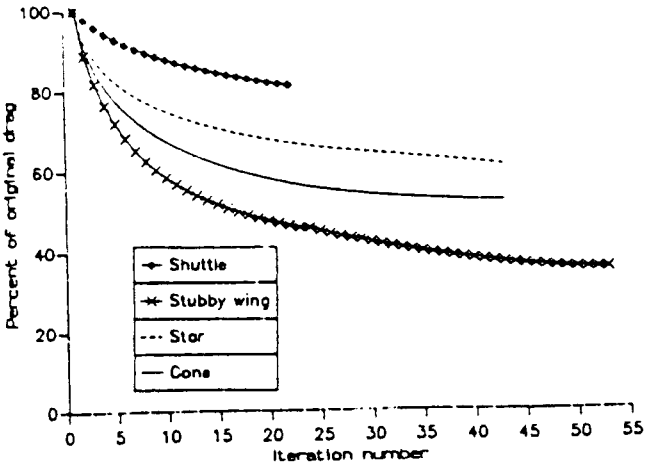

Figure 6. Convergence histories for four test shapes when using Fourier coefficient algorithm: normalized drag reduction.

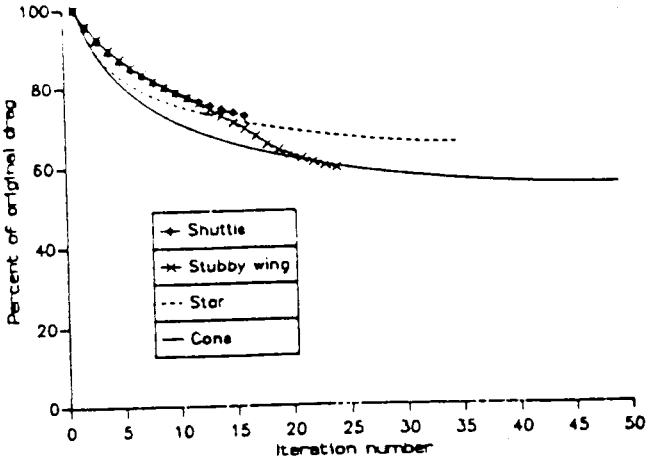

Figure 7. Convergence histories for four test shapes when using point-motion algorithm: normalized drag reduction.

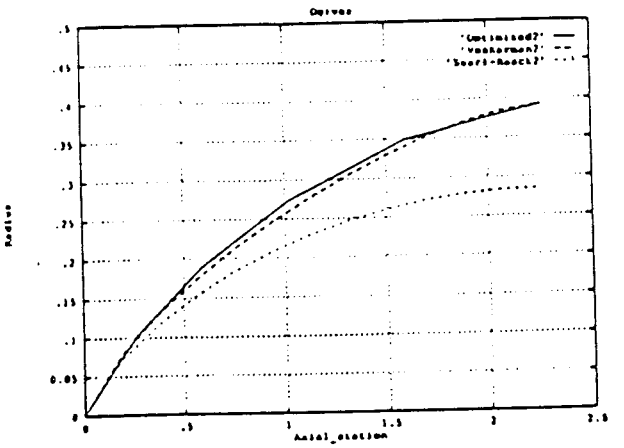

Figure 8. Comparison of analytically optimized ogives and a numerically optimized ogive using Fourier coefficient algorithm (inviscid computations).

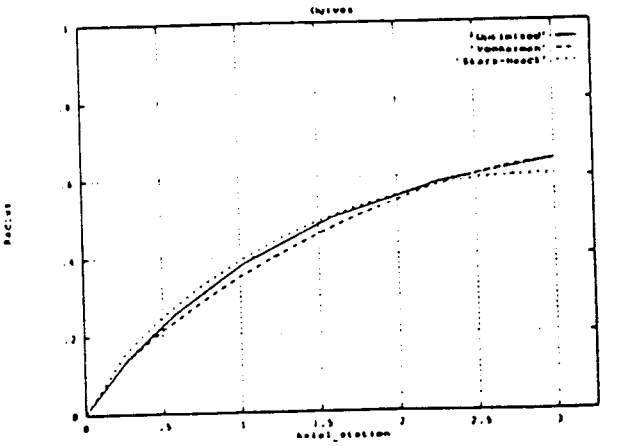

Figure 9. Comparison of analytically optimized ogives and a numerically optimized ogive using point-motion algorithm (inviscid computations).

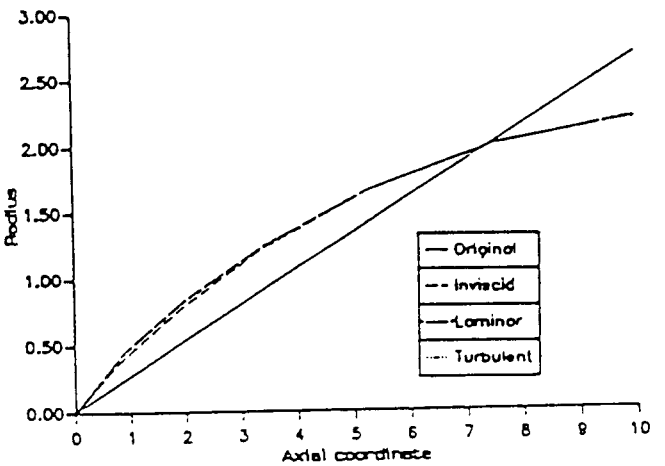

Figure 10. Comparison of the optimized ogive shapes with and without viscous effects.

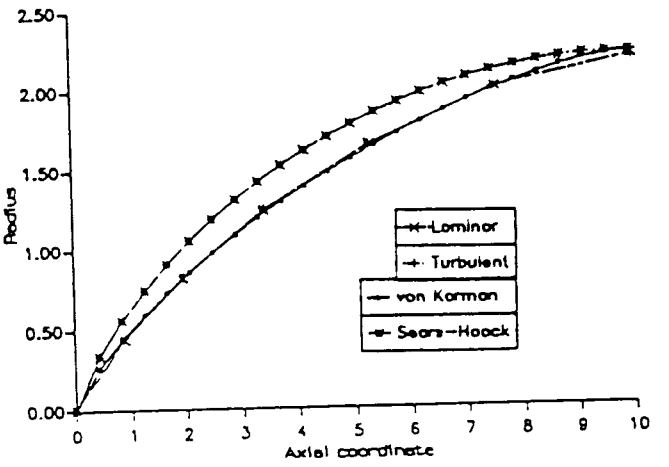

Figure 11. Comparison of viscous numerically optimized ogive shapes and analytically optimized ogives.

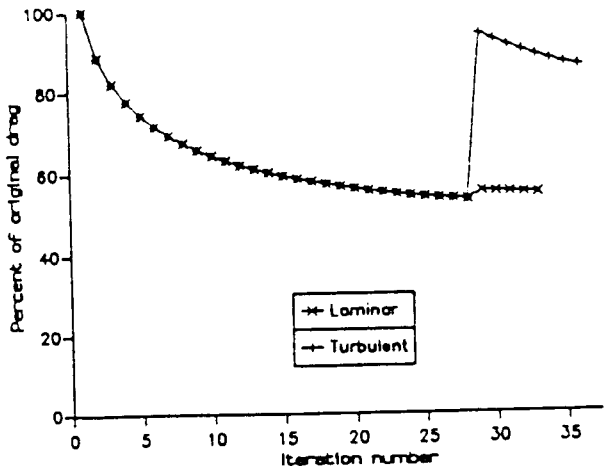

Figure 12. Convergence histories for initially inviscid normalized wave drag minimization that was later combined with boundary layer viscous effects.